THE JOURNAL OF PHYSICAL CHEMISTRY C

Article

Cite This: J. Phys. Chem. C XXXX, XXX, XXX−XXX

pubs.acs.org/JPCC

Manipulation of Phase-Transfer Ligand-Exchange Dynamics of PbS Quantum Dots for Efficient Infrared Photovoltaics

Lei Wang,[†] Yinglin Wang,*[,†] Yuwen Jia,[†] Xinlu Liu,[†] Ting Liu,[†] Ting Fu,[†] Jinhuan Li,[†] Binbin Weng,[‡] Xintong Zhang,*[,†] and Yichun Liu[†]

[†]Center for Advanced Optoelectronic Functional Materials Research, and Key Laboratory of UV Light-Emitting Materials and Technology of Ministry of Education, Northeast Normal University, Changchun 130024, Jilin, P. R. China

[‡]School of Electrical and Computer Engineering, University of Oklahoma, Norman, Oklahoma 73019, United States

Supporting Information

ABSTRACT: Chemical surface treatment of colloidal quantum dots (CQDs) by phase-transfer ligand-exchange (PTLE) is essential to implement highly densified, well-passivated CQD films for optoelectronic applications, such as infrared photovoltaics, light-emitting diodes, and photodetectors. PTLE, however, involves parallel and interactional processes of ligand exchange, phase transfer, and surface passivation of CQDs, which render the optimization of PTLE still challenging. Herein, we explored the action mechanism of a widely used additive, ammonium acetate (AA), on the PTLE of PbS CQDs to recognize the dynamic balance during the PTLE process and its impact on the performance of colloidal quantum dot solar cells (CQDSCs). Our research definitely shows that the AA additive can modify the dynamics of PTLE by participating in all of the three processes, and the amount of AA significantly influences the defect passivation and colloidal stability of PbS CQDs. At an appropriate concentration (~50 mM) of AA, PbS CQDs are well iodide-passivated by PTLE, and the fabricated CQDSCs achieve a power conversion efficiency (PCE) of ~10% associated with improved carrier transport and reduced trap-assisted carrier recombination. However, excessive AA causes trace residual AA on the CQD surface, resulting in the insufficient surface passivation of PbS CQDs and trap issues of CQDSCs. The double-edged sword effect of the AA additive on PTLE, demonstrated in our work, suggests that realizing a dynamic balance of different processes during PTLE is crucial for further performance promotion of CQDSCs.

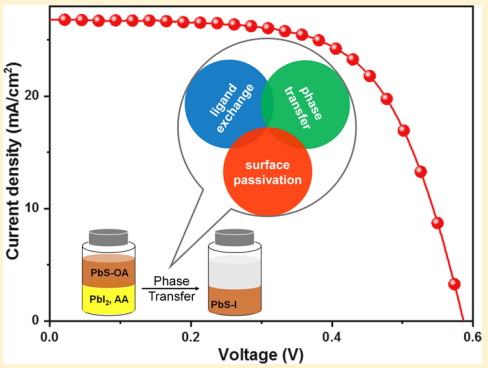

INTRODUCTION

Colloidal quantum dot solar cells (CQDSCs) based on lead chalcogenides (PbX; X = S, Se, or Te) could harvest solar photons in the range from the near- to mid-infrared region and possess advantages of size-tunable optical and electronic properties, good stability, and low-temperature solution processability.[1−6] This has led to CQDSCs emerging as outstanding candidates for the next-generation infrared photovoltaic and tandem photovoltaic devices to cover the absorption-edge shortage of crystalline silicon (1.1 eV) and perovskites (1.58 eV).[7−11] The principal process in the fabrication of CQDSCs involves the ligand exchange of the as-synthesized colloidal quantum dots (CQDs), which chemically replaces the highly insulating, long-chain oleic acid (OA) ligands by small ligands to promote the interdot electronic coupling in the CQD films.[2,5,12−14] Ligand exchange used to be performed in solid-state CQD films, leading to CQDSCs being associated with serious problems including an appreciable residual of long-chain ligands and material consumption.[10,15−18] Recently, a phase-transfer ligand-exchange (PTLE) strategy was developed to conveniently produce a high-concentration solution of inorganic-ligand-capped PbS CQDs.[5,7,19−21] It makes the fabrication of CQDSCs easy and dramatically promotes the photovoltaic performance of CQDSCs.[7,22−25] Consequently, the optimization of PTLE is of the essence for high-efficiency CQDSCs.

In the PTLE process, the replacement of the original long-chain ligands by inorganic ligands realizes the phase transfer of PbS CQDs. In addition, the inorganic ligands passivate surface traps of PbS CQDs generated during the synthesis of CQDs and the dissociation of long-chain ligands, which is of importance for reducing the trap-assisted recombination loss of CQDSCs.[10,12,14,26] The ligand exchange, phase transfer, and surface passivation of CQDs occur simultaneously during the PTLE process within a few minutes, and so it is reasonable that these three processes influence each other heavily. For example, although the strong passivation effect of inorganic PbI_2 ligands has been well proved, PTLE using sole PbI_2 ligands faces the issue of residual long-chain ligands.[10,14,18] This induces the incomplete phase transfer of PbS CQDs as well as poor colloidal stability of the PbS CQD solution, and leads to unexpected problems of carrier transport and

Received: September 30, 2019
Revised: November 19, 2019
Published: November 26, 2019

DOI: 10.1021/acs.jpcc.9b09231
J. Phys. Chem. C XXXX, XXX, XXX−XXX

recombination in CQDSCs.[27−29] These three processes easily become out-of-balance because of their different dynamic behaviors, and this makes the optimization of PTLE challenging and unpredictable.

Ammonium acetate (AA) is a widely used additive in the PTLE process of PbS CQDs.[5,14,17,27] However, its influence on the dynamics of PTLE remained controversial. Herein, we explored the action mechanism of AA on the PTLE process to recognize the dynamic balance among the ligand exchange, phase transfer, and surface-trap passivation. We demonstrated the great effect of residual AA, grafted on the surface of PbI_2-caped PbS CQDs, on the performance of CQDSCs for the first time. Even though AA efficiently accelerates the removal of original OA ligands, the trace residual of AA on the surface of PbS CQDs, induced by the high concentration of AA in the precursor solution, leads to the surface-trap issues of PbS CQDs. Consequently, PbS CQDSCs formed by high-concentration AA are faced with a serious trap-induced loss of carrier transport and recombination. In contrast, PbS CQDSCs formed by AA with an optimal concentration of 50 mM achieve a power conversion efficiency (PCE) in excess of 10% and a long-time air-storage stability. Our results described the two-step ligand exchange during the AA-assisted PTLE process, and the effect of the AA additive on the positive and negative sides. These results should be carefully considered in the further chemical modification of PTLE for the performance enhancement of PbS CQDSCs.

METHODS

Ligand Exchange of CQDs. The OA-capped PbS CQDs were synthesized by the hot-injection method as described in our previous publication.[11] The PTLE process of CQDs was executed under ambient conditions by the reported recipe with a slight modification.[5] PbI_2 (0.2 M) and $PbBr_2$ (0.04 M) and different concentrations of AA (0, 25, 50, 75 mM) were mixed and dissolved in *N*,*N*-dimethylformamide (DMF). PbS CQD octane solution (5 mL, 20 mg/mL) was blended with the lead halide solution for several minutes until the CQDs were completely transferred to the DMF solution. Then, the CQD solution was washed three times with octane. PbI_2-capped CQDs were precipitated with 3 mL of toluene and thereafter separated by centrifugation at 6000 rpm for 3 min. After 10 min of vacuum drying, CQDs were redispersed in butylamine (250 mg/mL) for CQD film deposition.

Device Fabrication. The sol−gel ZnO solution was spin-coated on the cleaned fluorine-doped tin oxide (FTO), and then the films were annealed at 200 °C for 30 min. CQD films were fabricated by single-step spin-coating at 2000 rpm for 30 s. For the PbS−EDT layers, the CQD octane solution (50 mg/mL) was spin-coated on the CQD film, then treated with EDT acetonitrile solution (0.02 vol %), and rinsed with acetonitrile. This procedure was repeated two times. Finally, Au electrodes (~100 nm) were deposited on the films by thermal evaporation. The active area (4.9 mm^2) of these devices was defined by a shadow mask.

Material and Device Characterization. UV−vis absorption spectra were studied using a UH4150 spectrophotometer. Steady-state photoluminescence (PL) spectra and PL decay data were recorded with Photon Technology HORIBA QM8000 with a cathode sensitive to near-IR radiation. The PL decay lifetimes were analyzed by fitting the curves through a single-exponential component. The current density−voltage curves of these devices were measured using a Keithley 2400 sourcemeter equipped with a 3A Steady-State Solar Simulator (Enli Technology Co., Ltd.). External quantum efficiency data (EQE) were obtained by a Zolix Instruments system equipped with a monochromatic illumination and a standard photodetector. Cross-sectional scanning electron microscopy (SEM) images of these samples were observed with a field-emission scanning electron microscope, FEI Quanta 250. Fourier transform infrared spectroscopy (FTIR) data were measured by a Thermo Fisher FTIR, Nicolet 6700. X-ray photoelectron spectroscopy (XPS) measurements were acquired using a Kratos AXIS ULTRA X-ray photoelectron spectroscope equipped with the Al Kα radiation. Transient photovoltage (TPV) measurements and charge-extraction characteristics were analyzed with a ModuLab XM Photoelectrochemical Test System (error estimates were calculated from more than four devices in each sample).

RESULTS AND DISCUSSION

The PTLE process of PbS CQDs is illustrated in Figure 1 and described in detail in the Methods. The *N*,*N*-dimethylformamide (DMF) solution, containing a lead halide complex and ammonium acetate (AA) with different concentrations (0, 25, 50, and 75 mM), was blended with the octane solution of PbS−OA CQDs (OA-caped PbS CQDs, Figure S1). After stirring for several minutes, the phase-transfer process was gradually accelerated along with the increase of AA concentration (Figure S2). However, PbI_2-capped CQDs were rapidly precipitated from DMF after the phase-transfer process when the precursor solution contained no or a low concentration (25 mM) of AA (the inset of Figure 1a). In contrast, when the concentration of AA increased to 50 mM, the PbS CQD solution could disperse well in the DMF solution. This phenomenon indicates that the AA additive can effectively improve the dispersibility of the CQD solution. Compared with the results of the PbS−OA CQD solution (Figure S1), the absorption and steady-state PL spectra of PbI_2-capped CQDs show slight red shifts of 22 and 36 nm, respectively. This red shift of the spectra is related to the variations of surface dipole and the quantum confinement effect, which are caused by the ligand exchange from OA to

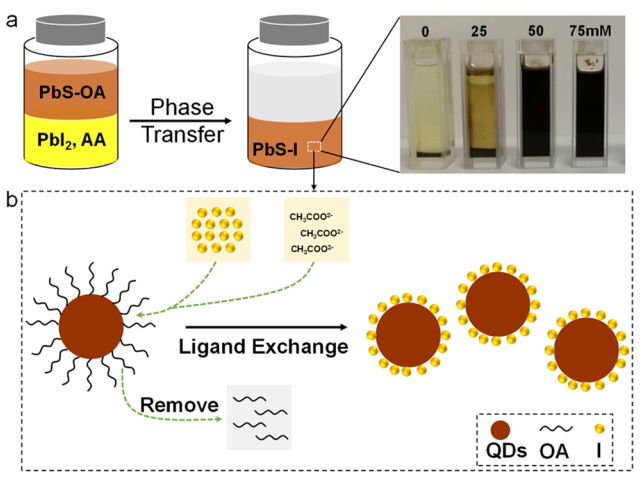

Figure 1. Schematic illustration of the phase-transfer ligand-exchange process for the CQD solution. (a) Phase-transfer process of CQDs (inset: photographs of CQD solution with different concentrations of AA); (b) AA-assisted phase-transfer ligand-exchange process.

DOI: 10.1021/acs.jpcc.9b09231
J. Phys. Chem. C XXXX, XXX, XXX−XXX

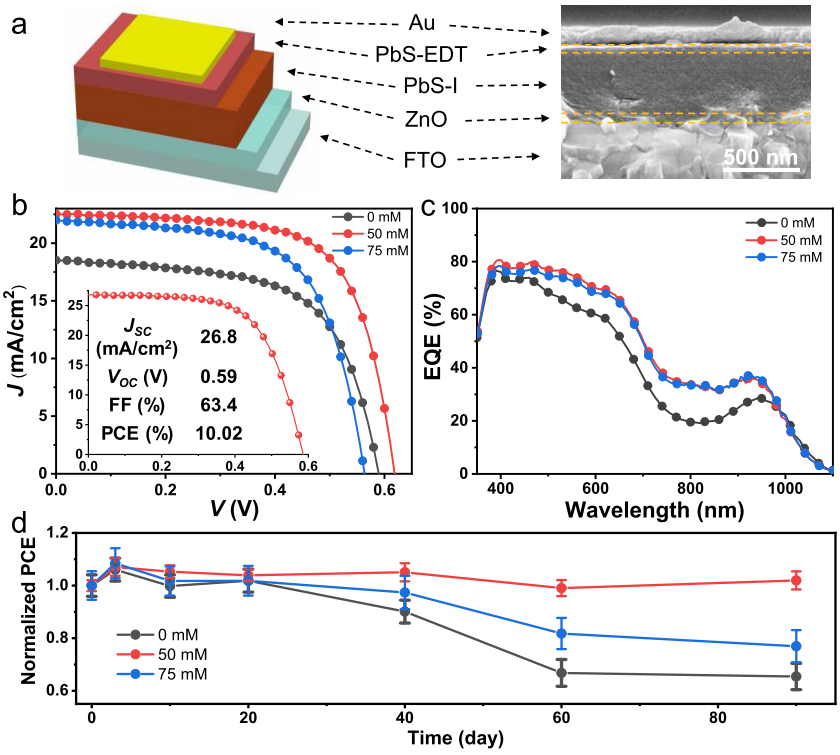

Figure 2. (a) Schematic structure and cross-sectional SEM image of the PbS CQD device. (b) Current−voltage (J−V) curves of devices formed with different concentrations of AA (inset: J−V curve of best-performance CQDSCs formed with an AA concentration of 50 mM). (c) External quantum efficiency spectra. (d) Air-storage stability variation of devices under an ambient atmosphere.

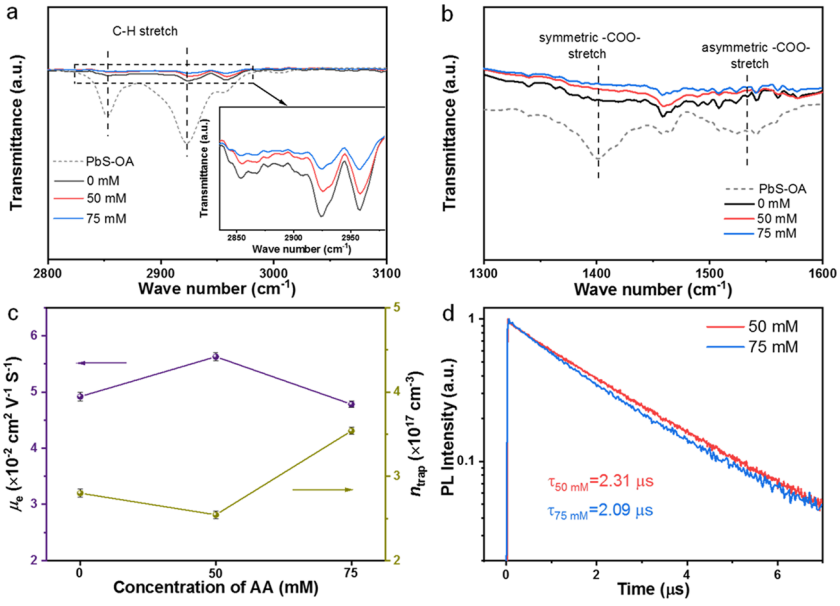

Figure 3. FTIR spectra of CQD films in the wavenumber ranges of (a) 2800−3100 cm^{-1} and (b) 1300−1600 cm^{-1}. (c) Electron mobility and trap density of PbS CQD films formed by different concentrations of AA. (d) PL decay traces of PbS CQDs treated with 50 and 75 mM AA in DMF solution.

PbI_2.[5,12,13] In addition, the half-peak-width of the PL peak shrinks from 112 to 92 nm after the PTLE process. This indicates an improved size-monodispersity of PbI_2-capped PbS CQDs. Furthermore, the PbI_2-capped and OA-capped CQDs reveal PL lifetimes of 2.31 and 3.65 μs, respectively. The shorter lifetime of PbI_2-capped CQDs is ascribed to the smaller size of PbI_2 inorganic ligands, which improved the electronic coupling between CQDs.[14,17,20] Finally, all of the ligand-exchanged CQDs were precipitated with toluene (an antisolvent). The obtained QDs were dissolved in butylamine for film deposition.

Photovoltaic devices were built and characterized to investigate the influence of the AA concentration. Figure 2a shows the schematic diagram and cross-sectional scanning electron microscopy (SEM) image of PbS CQDSCs with a device structure of FTO/ZnO/PbS−I/PbS−EDT-

DOI: 10.1021/acs.jpcc.9b09231
J. Phys. Chem. C XXXX, XXX, XXX−XXX

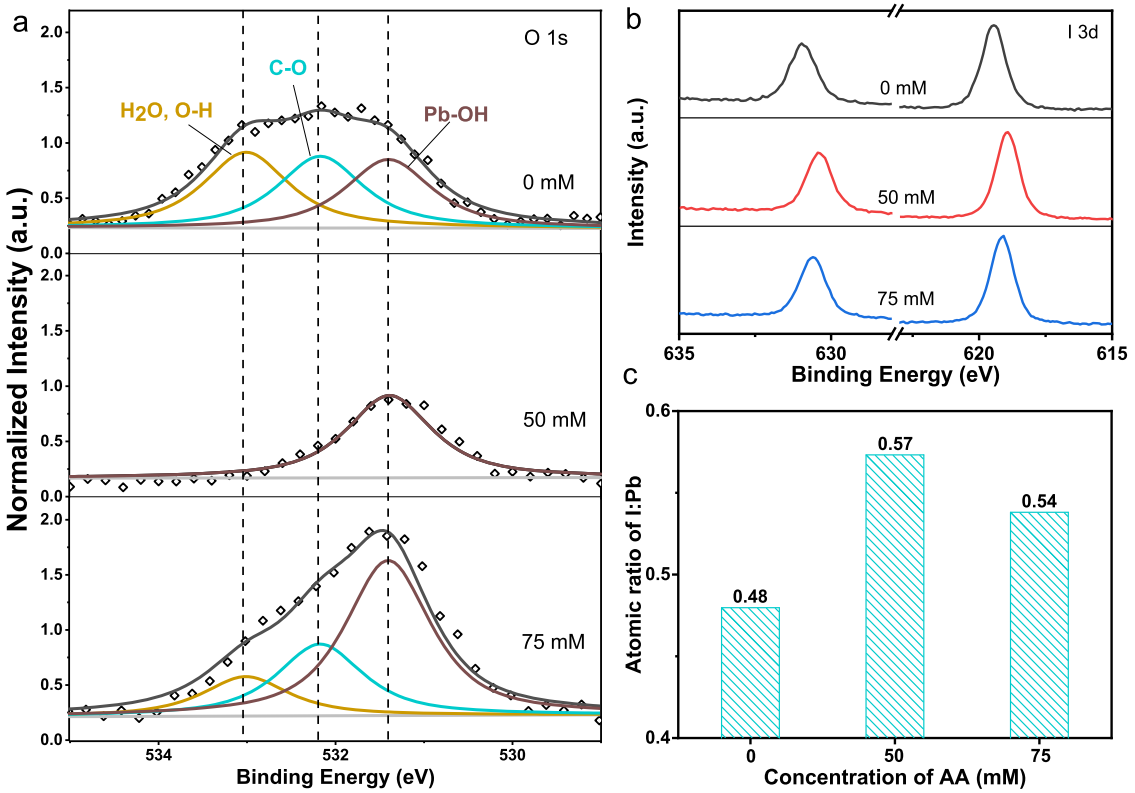

Figure 4. (a) O 1s signal peaks, (b) I 3d signal peaks, and (c) atomic ratio of I/Pb obtained from XPS spectra of PbS CQD films with different concentrations of AA.

(ethanedithiol)/Au. The current−voltage (J−V) curves of these devices under simulated AM 1.5G illumination (100 mW/cm^2) are plotted in Figure 2b. The statistical distribution of photovoltaic parameters is shown in Figure S3 and Table S1. The devices without AA reach a PCE of 6.69% generated by an open-circuit voltage (V_{oc}) of 0.58 V, a fill factor (FF) of 62.39%, and a short-circuit current density (J_{sc}) of 18.48 mA/cm^2. Increasing the concentration of AA to 50 mM dramatically enhances the PCE to 9.04% with the improved V_{oc} of 0.61 V, FF of 66.71%, and J_{sc} of 22.21 mA/cm^2. The PCE of the device with 50 mM AA could be further improved to 10.02% by a careful thickness optimization of PbS CQD light-harvesting films (the inset of Figures 2b and S4). However, further increase of the AA concentration to 75 mM negligibly changes the J_{sc}, but it obviously decreases the V_{oc} and FF values to 0.57 V and 62.68%, respectively, which leads to a suboptimal PCE of 7.61%. The compared external quantum efficiency spectra (EQE) of devices with AA concentrations of 50 and 75 mM (Figure 2c) also confirm that the efficiency difference between these two devices is mainly derived from the variation of V_{oc} and FF. We further monitored the air-storage stability of these devices with different AA concentrations (Figures 2d and S5). After 90 days of storing under ambient conditions, the device formed by 50 mM AA maintains ∼95% of its original PCE, whereas the PCE of the devices formed by 0 and 75 mM AA were decreased to 62 and 71%, respectively.

To explore the origin of the performance variation caused by AA, we first compared the variation of surface ligands caused by AA using the Fourier transform infrared spectra (FTIR, Figure 3a,b). The PbS CQD films formed without AA showed strong peaks of stretching vibrations for −CH_3, −CH_2, and −COO− groups, revealing the residual of OA after the PTLE process. In contrast, the signals of −CH_3 and −CH_2 related to the OA ligands reduced in sequence along with the increase of the AA concentration. In addition, the signals associated with the −COO− groups became hardly detectable in the CQD films prepared with the AA additive. These variations of the FTIR results caused by AA demonstrate that AA could accelerate the removal of the OA ligands. Previous literature has demonstrated that the exchange of insulating ligands by small molecules and/or inorganic ligands could enhance interdot electronic coupling and promote carrier transport in the CQD film.[10,16,30,31] In our work, we observed that the electron mobility (μ_e) of PbS CQD films increased from 4.92 × 10^{-2} to 5.63 × 10^{-2} cm^2/V S (Figures 3c and S6) when the AA concentration increased from 0 to 50 mA through the space-charge-limited current (SCLC) measurements.[28,32,33] This result further confirms the effect of removing the insulating ligands on the enhancement of carrier transport in the CQD films and is well-associated with the performance promotion of solar cells with an AA concentration of 50 mM. However, it is worthwhile to note that further increase of the AA concentration to 75 mM reduces the μ_e of the CQD film to 4.78 × 10^{-2} cm^2/V S despite the low residual amount of OA ligands in the 75 mM-AA-treated CQD films. In addition, the defect state density (n_{trap}) of an appropriate (50 mM) AA-treated CQD film is less than that of CQD films without AA (Figure 3c). However, a high concentration of AA (75 mM) dramatically exacerbates the n_{trap} of CQD films. Compared with the 75 mM-AA-treated CQD solution, furthermore, the CQD solution treated with 50 mM AA reveals a higher PL intensity and a larger decay lifetime (Figures 3d and S7). Consequently, there is no doubt that the increasing

DOI: 10.1021/acs.jpcc.9b09231
J. Phys. Chem. C XXXX, XXX, XXX−XXX

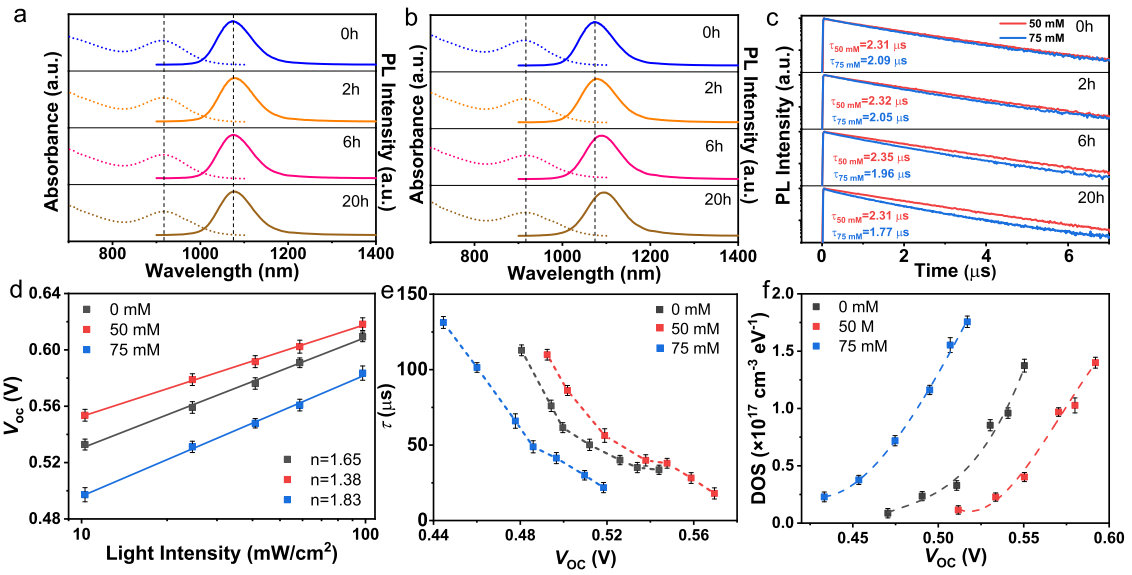

Figure 5. (a–c) Evolution of absorption, steady-state PL spectra, and PL decay with time in an ambient atmosphere for the CQD DMF solvent with 50 and 70 mM AA, respectively. (d) Light-intensity-dependent V_{ov} variation for different AA-treated CQD devices. (e) Carrier recombination time and (f) density of trap states of different AA-treated CQD devices from TPV and charge-extraction technology.

concentration of AA additive could efficiently decrease the residual of original OA ligands and enhance the interdot electronic coupling. However, an excess amount of AA may induce the trap generation of PbS CQD films.

X-ray photoelectron spectroscopy (XPS) was employed to explore the origin of trap-amount change caused by the AA concentration. The absence of the N 1s signal from XPS reveals that ammonium groups of AA are not absorbed on the PbS CQD surface (Figure S8). The O 1s spectra of PbS CQDs (Figure 4a) without AA can be resolved into three species, Pb–OH (533.30 eV), C–O (532.16 eV), and H_2O/OH (531.39 eV), as summarized in Table S2. Pb–OH, one of the sources leading to the sub-bandgap traps, is usually regarded as the hydroxyl ligand grafted on the surface of PbS CQDs.[34−36] The H_2O/OH groups are derived from the adsorbed oxygen species, which incline to interact with the surface defects of PbS CQDs. C–O species are assigned to the carboxyl group of OA ligands. When the concentration of AA increases to 50 mM, the absence of O 1s signals related to C–O and H_2O/OH of the CQD film demonstrates the promotional effect of AA on the removal of the original OA ligands and surface passivation of CQDs. However, along with the increase of the AA concentration up to 75 mM, the O 1s signal related to C–O and H_2O/OH emerges again on the PbS CQDs. Considering the weak signal of C–H groups obtained from FTIR results of CQD films formed by AA, the C–O signal on the CQD film treated with 75 mM AA could not be derived from the residual original OA ligands, but it may be associated with the trace residual of AA additives. These remaining AA additives will influence the combination of PbI_2 with CQDs. The I 3d peaks of PbS CQD films formed by 50 mM AA present the lowest binding energy compared with those of films formed from 0 to 75 mM AA (Figure 4b), suggesting the strongest interaction between I and Pb on the PbS CQD surface among three samples.[36,37] Moreover, the largest atomic ratio of I/Pb is also observed when the AA concentration is 50 mM (Figure 4c). The higher I/Pb atomic ratio indicates a better surface passivation of PbS CQDs. These results indicate that adopting a high concentration of AA additive during the PTLE process will induce the trace residual of AA, weaken the interaction between PbI_2 ligands and CQDs, and decrease the amount of PbI_2 on the CQD surface.

Based on the observed results, we could propose the influence mechanism of AA concentration on the PTLE process (Figure 1b). The stability constant (β_n) of Pb^{2+} and acetate groups is larger than that of Pb^{2+} and I^-, which implies that the AA additive could combine with the surface of PbS CQDs more easily than I^- during the ligand-exchange process.[38] This preferential combination between acetate groups of AA and PbS CQDs reduces the steric hindrance on the surface of CQDs caused by the original OA ligands.[18,39] Since the concentration of PbI_2 ligands is much larger than that of the AA additive, the grafted AA will finally be exchanged by PbI_2.[34] Therefore, we observed negligible signals related to AA when the AA concentration was 50 mM. This leads to a superior surface passivation of the PbS CQD solution. However, excess AA during the PTLE process can result in the residual of acetate groups, which could not be completely exchanged by PbI_2 and decrease the amount of PbI_2 on the CQD surface. Since acetate groups have been reported to present a weaker trap-passivation effect than halides, this trace residual of AA may cause the inferior surface passivation of CQDs and trap issues. To verify the hypothesis, we introduced a large amount of AA (200 mM) in the DMF phase for the PTLE process of the PbS CQD solution. A larger Stokes shift is observed as shown in Figure S9a. From the FTIR spectra (Figure S9b), the features of antisymmetric and symmetric carboxylate stretching vibrations significantly increase for the 200 mM-AA-treated CQDs, which may be attributed to the residual acetate groups. The O 1s signal spectra of CQDs with 200 mM AA show significantly increased hydroxyl ligands (Pb–OH), which suggest enormous surface defects of CQDs (Figure S9c). These results indicate that acetate groups participate in the ligand-exchange process, and excess AA can lead to the residual acetate on the CQD surface.

The influence of high-concentration AA was further investigated by the time-dependent absorption and photoluminescence (PL) spectra of the PbS CQDs in DMF solution

DOI: 10.1021/acs.jpcc.9b09231
J. Phys. Chem. C XXXX, XXX, XXX–XXX

(Figure 5a,b). The first exciton absorption peaks of CQD solutions formed by 50 and 75 mM AA are both located at 916 nm. These peaks remain unchanged over 20 h. The PL peaks of the CQD solution formed by 50 mM AA show almost identical emission peaks at 1076 nm and thus generate constant Stokes shifts of ∼160 nm over 20 h (Figure S10). However, the emission peak of the CQD solution formed by 75 mM AA gradually red shifts from 1076 to 1094 nm along with the increase of the standing time. Accordingly, this red shift leads to an increased Stokes shift from 160 to 178 nm. In addition, compared with the constant PL lifetime (τ, ∼ 2.31 μs) of the CQD solution formed by 50 mM AA with different standing times, the τ of the CQD solution with 75 mM AA decreases from 2.09 to 1.77 μs along with the increase of the standing time (Figure 5c). Since acetate groups have been reported to present a weaker trap-passivation effect than halides, the trace residual of AA on the CQD surface, when the concentration of AA is 75 mM, may cause the inferior surface passivation of CQDs and trap issues. Consequently, we ascribe the shorter τ of the CQD solution with 75 mM AA to the aggravated trap-assisted nonradiative decay rate of photogenerated carriers. Furthermore, the inferior surface passivation of PbS CQDs could induce the adsorption of oxygen/water on the CQD surface. This could be correlated well with the observed instability of the device formed by 75 mM AA as shown in Figure 2. In addition, we further increased the storing time of the PbS CQD solution treated with a the lower concentration (50 mM). With a storing time of 40 h, spectra of the PbS CQD solution treated with 50 mM AA show a negligible change compared with the initial one (Figure S11). This indicates the good stability of CQDs formed by 50 mM AA. These steady and transient PL results indicate that the CQD solution formed by an appropriate AA concentration presents considerable stability; nevertheless, insufficient surface passivation of CQDs, caused by high-concentration AA, could reduce the stability of CQDs and induce more serious trap-induced nonradiative recombination after long-time standing.

To further verify the influence of the AA concentration on the photovoltaic performance, the dependences of V_{oc} and J_{sc} on the light intensity (I) were measured (Figures 5d and S12).[40] The relation between V_{oc} and I can be expressed as $V_{oc} = (nkT/q)\ln(I) + C$, where n, k, T, and q are the ideality factor, Boltzmann constant, Kelvin temperature, and elementary charge, respectively.[40] The n values of these devices with 0, 50, and 75 mM AA are estimated to be 1.65, 1.38, and 1.83, respectively. n values of 1 and 2 indicate that the dominant recombinations of the device under open-circuit conditions are the band-to-band and trap-related processes, respectively. Therefore, the lower n value of the device with 50 mM AA manifests a decreased trap-related recombination of solar cells caused by the sufficient surface passivation of PbS CQDs. However, the increased n value of the device with 75 mM AA suggests the exacerbated trap-related recombination. This could be correlated well with the serious trap issues of PbS CQDs caused by the trace residual of AA. The variation of the exponential factor α calculated from the light-intensity dependence of J_{sc} also indicates a suppressed carrier recombination under the short-circuit condition for the solar cell formed by 50 mM AA (Figure S12). The carrier recombination times (τ_r) extracted from transient photovoltage (TPV) measurements under different background light intensities are displayed in Figure 5e.[19,40] The τ_r of the device treated with 50 mM AA is larger than those of devices with 0 and 75 mM AA, resulting in a suppressed recombination loss. These results of carrier recombination times are highly consistent with the variation of n values. Furthermore, the density of states (DOS) of these devices were extracted by charge-extraction technology (Figure 5f).[41] The device with 50 mM AA has a lower DOS compared to the device without AA. However, the DOS obviously increases when AA is excessive. The above characterizations of carrier recombination and trap states indicate that the appropriate concentration (∼50 mM) of AA can effectively reduce the defect states and inhibit carrier recombination, and thus improve the V_{oc} of the device due to the efficient surface passivation of CQDs. Nevertheless, the unexpected traps induced by excess AA lead to additional carrier recombination processes.

The recognition of the action mechanism of a widely used additive (AA) on the PTLE process is essential for the high-throughput deposition of densified, well-passivated CQD films. Recently, various high-performance PbS CQD-based optoelectronic devices, such as photodetectors and field-effect transistors, have been fabricated by the PTLE method.[42,43] Consequently, our research is of importance for further improvement of these CQD-based optical and/or electronic devices.

CONCLUSIONS

In summary, we have explored the influence of the AA additive on the phase-transfer ligand exchange of CQDs by manipulating the concentration of the AA additive. AA can effectively accelerate the removal of oleic acid ligands, but it is worthwhile to notice that the control of the AA residual amount on the PbI_2-capped PbS CQDs is of importance for the performance of CQDSCs. AA grafted on the PbS surface could be replaced by PbI_2. This leads to superior iodide-passivated PbS CQDs and improved colloidal stability of the CQD solution. Consequently, the PbS CQD device formed with the appropriate concentration (50 mM) of AA achieves a PCE of ∼10%, which is associated with an improved carrier transport and reduced trap-assisted carrier recombination. However, a high concentration of AA during PTLE results in residual ammonium groups on the PbS surface. This causes insufficient surface passivation of PbS CQDs and trap issues of CQDSCs. Our work demonstrates the double-edged sword effects of the additive on the PTLE process and suggests that the complicated relation among ligand exchange, phase transfer, and trap passivation should be carefully controlled for further optimization of PTLE.

ASSOCIATED CONTENT

Supporting Information

The Supporting Information is available free of charge at https://pubs.acs.org/doi/10.1021/acs.jpcc.9b09231.

Experimental section; absorption and PL spectra and PL decay for PbS−OA CQD and PbI_2-capped CQD solution with 50 mM AA; photographs of the PTLE process for CQDs with different concentrations of AA; statistical distribution of photovoltaic parameters for 24 devices; detailed photovoltaic parameters of CQD devices with different concentrations of AA; PCE as a function of the thickness of the PbS−PbI_2 CQD film; EQE of the device with a CQD film thickness of 380 nm; air-storage stability of devices with different concentrations of AA under ambient conditions; $I-V$

DOI: 10.1021/acs.jpcc.9b09231
J. Phys. Chem. C XXXX, XXX, XXX−XXX

curves for electron-type CQD devices; steady-state PL spectra of the PbS CQD solutions treated with 50 and 75 mM AA in DMF solution; N 1s of XPS spectra for CQD films; fitting parameters and quantitative analysis of O 1s spectra of PbS CQDs with different concentrations of AA; absorption and PL spectra, FTIR spectra of CQD solution treated with 75 and 200 mM AA, and O 1s signal speaks of XPS spectra for CQDs with 200 mM AA; change of the Stokes shift with time for CQD solution treated with 50 and 75 mM AA; absorption and PL spectra and PL decay for CQDs formed by 50 mM AA over 0 and 40 h; light-intensity-dependent J_{sc} variation for different AA-treated CQD devices (PDF)

AUTHOR INFORMATION

Corresponding Authors

*E-mail: wangyl100@nenu.edu.cn (Y.W.).
*E-mail: xtzhang@nenu.edu.cn (X.Z.).

ORCID

Xintong Zhang: 0000-0003-0561-8902

Notes

The authors declare no competing financial interest.

ACKNOWLEDGMENTS

This work was supported by the Natural Science Foundation of China (91833303, 51872044, 51602047, and 51372036), the Key Project of Chinese Ministry of Education (113020A), the 111 project (B13013), and Jilin Scientific and Technological Development Program (20180520007JH).

REFERENCES

(1) Tang, J.; Brzozowski, L.; Barkhouse, D. A. R.; Wang, X.; Debnath, R.; Wolowiec, R.; Palmiano, E.; Levina, L.; Pattantyus-Abraham, A. G.; Jamakosmanovic, D.; et al. Quantum Dot Photovoltaics in the Extreme Quantum Confinement Regime: The Surface-Chemical Origins of Exceptional Air- and Light-Stability. *ACS Nano* **2010**, *4*, 869−878.

(2) Chuang, C.-H. M.; Brown, P. R.; Bulović, V.; Bawendi, M. G. Improved Performance and Stability in Quantum Dot Solar Cells through Band Alignment Engineering. *Nat. Mater.* **2014**, *13*, 796−801.

(3) Zhang, J.; Gao, J.; Miller, E. M.; Luther, J. M.; Beard, M. C. Diffusion-Controlled Synthesis of PbS and PbSe Quantum Dots with in Situ Halide Passivation for Quantum Dot Solar Cells. *ACS Nano* **2014**, *8*, 614−622.

(4) Tang, J.; Kemp, K. W.; Hoogland, S.; Jeong, K. S.; Liu, H.; Levina, L.; Furukawa, M.; Wang, X.; Debnath, R.; Cha, D.; et al. Colloidal-Quantum-Dot Photovoltaics using Atomic-Ligand Passivation. *Nat. Mater.* **2011**, *10*, 765−771.

(5) Liu, M.; Voznyy, O.; Sabatini, R.; de Arquer, F. P. G.; Munir, R.; Balawi, A. H.; Lan, X.; Fan, F.; Walters, G.; Kirmani, A. R.; et al. Hybrid Organic−Inorganic Inks Flatten the Energy Landscape in Colloidal Quantum Dot Solids. *Nat. Mater.* **2017**, *16*, 258−263.

(6) Wang, H.; Gonzalez-Pedro, V.; Kubo, T.; Fabregat-Santiago, F.; Bisquert, J.; Sanehira, Y.; Nakazaki, J.; Segawa, H. Enhanced Carrier Transport Distance in Colloidal PbS Quantum-Dot-Based Solar Cells Using ZnO Nanowires. *J. Phys. Chem. C* **2015**, *119*, 27265−27274.

(7) Xu, J.; Voznyy, O.; Liu, M.; Kirmani, A. R.; Walters, G.; Munir, R.; Abdelsamie, M.; Proppe, A. H.; Sarkar, A.; de Arquer, F. P. G.; et al. 2D Matrix Engineering for Homogeneous Quantum Dot Coupling in Photovoltaic Solids. *Nat. Nanotechnol.* **2018**, *13*, 456−462.

(8) Wang, H.; Kubo, T.; Nakazaki, J.; Segawa, H. Solution-Processed Short-Wave Infrared PbS Colloidal Quantum Dot/ZnO Nanowire Solar Cells Giving High Open-Circuit Voltage. *ACS Energy Lett.* **2017**, *2*, 2110−2117.

(9) Baek, S.-W.; Ouellette, O.; Jo, J. W.; Choi, J.; Seo, K.-W.; Kim, J.; Sun, B.; Lee, S.-H.; Choi, M.-J.; Nam, D.-H.; et al. Infrared Cavity-Enhanced Colloidal Quantum Dot Photovoltaics Employing Asymmetric Multilayer Electrodes. *ACS Energy Lett.* **2018**, *3*, 2908−2913.

(10) Jo, J. W.; Choi, J.; García de Arquer, F. P.; Seifitokaldani, A.; Sun, B.; Kim, Y.; Ahn, H.; Fan, J.; Quintero-Bermudez, R.; Kim, J.; et al. Acid-Assisted Ligand Exchange Enhances Coupling in Colloidal Quantum Dot Solids. *Nano Lett.* **2018**, *18*, 4417−4423.

(11) Wang, L.; Jia, Y.; Wang, Y.; Zang, S.; Wei, S.; Li, J.; Zhang, X. Defect Passivation of Low-Temperature Processed ZnO Electron Transport Layer with Polyethylenimine for PbS Quantum Dot Photovoltaics. *ACS Appl. Energy Mater.* **2019**, *2*, 1695−1701.

(12) Beygi, H.; Sajjadi, S. A.; Babakhani, A.; Young, J. F.; Veggel, F. C. J. M. Halide-, Hybrid-, and Perovskite-Functionalized Light Absorbing Quantum Materials of P−i−n Heterojunction Solar Cells. *ACS Appl. Mater. Interfaces* **2018**, *10*, 30283−30295.

(13) Dirin, D. N.; Dreyfuss, S.; Bodnarchuk, M. I.; Nedelcu, G.; Papagiorgis, P.; Itskos, G.; Kovalenko, M. V. Lead Halide Perovskites and Other Metal Halide Complexes as Inorganic Capping Ligands for Colloidal Nanocrystals. *J. Am. Chem. Soc.* **2014**, *136*, 6550−6553.

(14) Zhang, X.; Zhang, J.; Phuyal, D.; Du, J.; Tian, L.; Öberg, V. A.; Johansson, M. B.; Cappel, U. B.; Karis, O.; Liu, J.; et al. Inorganic CsPbI3 Perovskite Coating on PbS Quantum Dot for Highly Efficient and Stable Infrared Light Converting Solar Cells. *Adv. Energy Mater.* **2018**, *8*, No. 1702049.

(15) Wang, R.; Shang, Y.; Kanjanaboos, P.; Zhou, W.; Ning, Z.; Sargent, E. H. Colloidal Quantum Dot Ligand Engineering for High Performance Solar Cells. *Energy Environ. Sci.* **2016**, *9*, 1130−1143.

(16) Kim, B.-S.; Hong, J.; Hou, B.; Cho, Y.; Sohn, J. I.; Cha, S.; Kim, J. M. Inorganic-Ligand Exchanging Time Effect in PbS Quantum Dot Solar Cell. *Appl. Phys. Lett.* **2016**, *109*, No. 063901.

(17) Jo, J. W.; Kim, Y.; Choi, J.; de Arquer, F. P. G.; Walters, G.; Sun, B.; Ouellette, O.; Kim, J.; Proppe, A. H.; Quintero-Bermudez, R.; et al. Enhanced Open-Circuit Voltage in Colloidal Quantum Dot Photovoltaics via Reactivity-Controlled Solution-Phase Ligand Exchange. *Adv. Mater.* **2017**, *29*, No. 1703627.

(18) Liu, M.; Che, F.; Sun, B.; Voznyy, O.; Proppe, A.; Munir, R.; Wei, M.; Quintero-Bermudez, R.; Hu, L.; Hoogland, S.; et al. Controlled Steric Hindrance Enables Efficient Ligand Exchange for Stable, Infrared-Bandgap Quantum Dot Inks. *ACS Energy Lett.* **2019**, *4*, 1225−1230.

(19) Aqoma, H.; Al Mubarok, M.; Hadmojo, W. T.; Lee, E.-H.; Kim, T.-W.; Ahn, T. K.; Oh, S.-H.; Jang, S.-Y. High-Efficiency Photovoltaic Devices using Trap-Controlled Quantum-Dot Ink prepared via Phase-Transfer Exchange. *Adv. Mater.* **2017**, *29*, No. 1605756.

(20) Kim, S.; Noh, J.; Choi, H.; Ha, H.; Song, J. H.; Shim, H. C.; Jang, J.; Beard, M. C.; Jeong, S. One-Step Deposition of Photovoltaic Layers Using Iodide Terminated PbS Quantum Dots. *J. Phys. Chem. Lett.* **2014**, *5*, 4002−4007.

(21) Balazs, D. M.; Rizkia, N.; Fang, H.-H.; Dirin, D. N.; Momand, J.; Kooi, B. J.; Kovalenko, M. V.; Loi, M. A. Colloidal Quantum Dot Inks for Single-Step-Fabricated Field-Effect Transistors: The Importance of Postdeposition Ligand Removal. *ACS Appl. Mater. Interfaces* **2018**, *10*, 5626−5632.

(22) Choi, M.-J.; Kim, Y.; Lim, H.; Alarousu, E.; Adhikari, A.; Shaheen, B. S.; Kim, Y. H.; Mohammed, O. F.; Sargent, E. H.; Kim, J. Y.; et al. Tuning Solute-Redistribution Dynamics for Scalable Fabrication of Colloidal Quantum-Dot Optoelectronics. *Adv. Mater.* **2019**, *31*, No. 1970225.

(23) Aqoma, H.; Jang, S.-Y. Solid-State-Ligand-Exchange Free Quantum Dot Ink-Based Solar Cells with an Efficiency of 10.9%. *Energy Environ. Sci.* **2018**, *11*, 1603−1609.

(24) Zhang, X.; Santra, P. K.; Tian, L.; Johansson, M. B.; Rensmo, H.; Johansson, E. M. J. Highly Efficient Flexible Quantum Dot Solar Cells with Improved Electron Extraction Using MgZnO Nanocrystals. *ACS Nano* **2017**, *11*, 8478−8487.

DOI: 10.1021/acs.jpcc.9b09231
J. Phys. Chem. C XXXX, XXX, XXX−XXX

(25) Kim, Y.; Che, F.; Jo, J. W.; Choi, J.; García de Arquer, F. P.; Voznyy, O.; Sun, B.; Kim, J.; Choi, M.-J.; et al. A Facet-Specific Quantum Dot Passivation Strategy for Colloid Management and Efficient Infrared Photovoltaics. *Adv. Mater.* **2019**, *31*, No. 1805580.
(26) Lin, Q.; Yun, H. J.; Liu, W.; Song, H.-J.; Makarov, N. S.; Isaienko, O.; Nakotte, T.; Chen, G.; Luo, H.; Klimov, V. I.; et al. Phase-Transfer Ligand Exchange of Lead Chalcogenide Quantum Dots for Direct Deposition of Thick, Highly Conductive Films. *J. Am. Chem. Soc.* **2017**, *139*, 6644−6653.
(27) Kim, J.; Ouellette, O.; Voznyy, O.; Wei, M.; Choi, J.; Choi, M.-J.; Jo, J. W.; Baek, S.-W.; Fan, J.; Saidaminov, M. I.; et al. Butylamine-Catalyzed Synthesis of Nanocrystal Inks Enables Efficient Infrared CQD Solar Cells. *Adv. Mater.* **2018**, *30*, No. 1803830.
(28) Gu, M.; Wang, Y.; Yang, F.; Lu, K.; Xue, Y.; Wu, T.; Fang, H.; Zhou, S.; Zhang, Y.; Ling, X.; et al. Stable PbS Quantum Dot Ink for Efficient Solar Cells by Solution-Phase Ligand Engineering. *J. Mater. Chem. A* **2019**, *7*, 15951−15959.
(29) Sayevich, V.; Gaponik, N.; Plötner, M.; Kruszynska, M.; Gemming, T.; Dzhagan, V. M.; Akhavan, S.; Zahn, D. R. T.; Demir, H. V.; Eychmüller, A. Stable Dispersion of Iodide-Capped PbSe Quantum Dots for High-Performance Low-Temperature Processed Electronics and Optoelectronics. *Chem. Mater.* **2015**, *27*, 4328−4337.
(30) Ip, A. H.; Thon, S. M.; Hoogland, S.; Voznyy, O.; Zhitomirsky, D.; Debnath, R.; Levina, L.; Rollny, L. R.; Carey, G. H.; Fischer, A.; et al. Hybrid Passivated Colloidal Quantum Dot Solids. *Nat. Nanotechnol.* **2012**, *7*, 577−582.
(31) Sun, B.; Voznyy, O.; Tan, H.; Stadler, P.; Liu, M.; Walters, G.; Proppe, A. H.; Liu, M.; Fan, J.; Zhuang, T.; et al. Pseudohalide-Exchanged Quantum Dot Solids Achieve Record Quantum Efficiency in Infrared Photovoltaics. *Adv. Mater.* **2017**, *29*, No. 1700749.
(32) Zhou, S.; Liu, Z.; Wang, Y.; Lu, K.; Yang, F.; Gu, M.; Xu, Y.; Chen, S.; Ling, X.; Zhang, Y.; et al. Towards Scalable Synthesis of High-Quality PbS Colloidal Quantum Dots for Photovoltaic Applications. *J. Mater. Chem. C* **2019**, *7*, 1575−1583.
(33) Speirs, M. J.; Dirin, D. N.; Abdu-Aguye, M.; Balazs, D. M.; Kovalenko, M. V.; Loi, M. A. Temperature Dependent Behaviour of Lead Sulfide Quantum Dot Solar Cells and Films. *Energy Environ. Sci.* **2016**, *9*, 2916−2924.
(34) Wang, Y.; Lu, K.; Han, L.; Liu, Z.; Shi, G.; Fang, H.; Chen, S.; Wu, T.; Yang, F.; Gu, M.; et al. In Situ Passivation for Efficient PbS Quantum Dot Solar Cells by Precursor Engineering. *Adv. Mater.* **2018**, *30*, No. 1704871.
(35) Cao, Y.; Stavrinadis, A.; Lasanta, T.; So, D.; Konstantatos, G. The Role of Surface Passivation for Efficient and Photostable PbS Quantum Dot Solar Cells. *Nat. Energy* **2016**, *1*, No. 16035.
(36) Song, J. H.; Choi, H.; Kim, Y.-H.; Jeong, S. High Performance Colloidal Quantum Dot Photovoltaics by Controlling Protic Solvents in Ligand Exchange. *Adv. Energy Mater.* **2017**, *7*, No. 1700301.
(37) Lan, X.; Voznyy, O.; Kiani, A.; García de Arquer, F. P.; Abbas, A. S.; Kim, G.-H.; Liu, M.; Yang, Z.; Walters, G.; Xu, J.; et al. Passivation Using Molecular Halides Increases Quantum Dot Solar Cell Performance. *Adv. Mater.* **2016**, *28*, 299−304.
(38) Meties, L. *Handbook of Analytical Chemistry*; McGraw-Hill, 1963; pp 318−320.
(39) Zarghami, M. H.; Liu, Y.; Gibbs, M.; Gebremichael, E.; Webster, C.; Law, M. p-Type PbSe and PbS Quantum Dot Solids Prepared with Short-Chain Acids and Diacids. *ACS Nano* **2010**, *4*, 2475−2485.
(40) Chuang, C.-H. M.; Maurano, A.; Brandt, R. E.; Hwang, G. W.; Jean, J.; Buonassisi, T.; Bulović, V.; Bawendi, M. G. Open-Circuit Voltage Deficit, Radiative Sub-Bandgap States, and Prospects in Quantum Dot Solar Cells. *Nano Lett.* **2015**, *15*, 3286−3294.
(41) Stavrinadis, A.; Pradhan, S.; Papagiorgis, P.; Itskos, G.; Konstantatos, G. Suppressing Deep Traps in PbS Colloidal Quantum Dots via Facile Iodide Substitutional Doping for Solar Cells with Efficiency > 10%. *ACS Energy Lett.* **2017**, *2*, 739−744.
(42) Sliz, R.; Lejay, M.; Fan, J. Z.; Choi, M.; Kinge, S.; Hoogland, S.; Fabritius, T.; García de Arquer, F. P.; Sargent, E. H. Stable Colloidal Quantum Dot Inks Enable Inkjet-Printed High-Sensitivity Infrared Photodetectors. *ACS Nano* **2019**, *13*, 11988−11995.
(43) Balazs, D. M.; Rizkia, N.; Fang, H.; Dirin, D. N.; Momand, J.; Kooi, B. J.; Kovalenko, M. V.; Loi, M. A. Colloidal Quantum Dot Inks for Single-Step-Fabricated Field-Effect Transistors: The Importance of Postdeposition Ligand Removal. *ACS Appl. Mater. Interfaces* **2018**, *10*, 5626−5632.

DOI: 10.1021/acs.jpcc.9b09231
J. Phys. Chem. C XXXX, XXX, XXX−XXX